CHAPTER 189

NUMERICAL MODEL FOR DENSITY CURRENTS IN ESTUARIES

Karsten Fischer*

1. Introduction

*

In the estuarine mixing areas of salt water and fresh water the vertical stream velocity profile generally is strongly affected by the baroclinic forces, giving rise to upstream currents near the bottom. Such reverse currents occur not only in stratified estuaries, but also in estuaries of the well-mixed type |1|, and they may cause problems like strong shoaling areas, salt intrusion, or difficulties when disposing wastes or dredged material 3. The contributions of the salinity variations to the tidal motion are comparable to the contributions from the fresh water upland discharge [1]. For well-mixed estuaries with negligible fresh water discharge, the tidal velocities and water elevations may be obtained from numerical vertically averaged models or from physical homogeneous-flow models, but for all other conditions or desired results one has to use numerical vertically discretized models or physical inhomogeneous-flow models. As numerical and physical models have different properties and deficiencies, they may be used complementarily rather than concurrently |4|, the farfield regime apparently becoming the domain of numerical models.

The increased public and scientific interest in water quality problems led to the development and application of baroclinic numerical tidal models |5, 6|. The present paper is concerned with the question, how well the action of baroclinic forces can be represented by numerical techniques. As a test example, the salt wedge problems is tackled. Studies on salt wedges by means of physical models have been very successful |1, 7|, but mathematical approches were confined to analytical solutions for the stationary salt wedge |8 - 10| and simple geometric boundaries only. The numerical approach is free from these restrictions, giving a solution of the complete equations of motion, continuity, and convection-diffusion simultaneously.

The main difficulty for the numerical model lies in the solution of the convection equation. The usual methods to solve the convection equation (like Forward Time / Centered Space, Upstream Differences, Lax-Wendroff, ADI, Leapfrog, or Galerkin-Finite Elements) break down when the convection of fairly sharp density jumps is to be calculated, as is the case for the salt wedge. Strong artificial diffusivity, mass losses, violations of the second law of thermodynamics or even unstable solutions are encountered. The numerical errors can be reduced considerably be using higher order difference approximations |11| at

Research Scientist, Sonderforschungsbereich 79, Technische Universität Hannover, F.R. Germany the expense of higher numerical effort and more complicated boundary conditions, or by using a floating (Lagrangian) grid formulation; however, shearing and circulating flow forces the programmer to interpolate back to a fixed (Eulerian) grid from time to time, so that the advantage of the Lagrangian formulation in part gets lost, while the full numerical effort remains. In the baroclinic numerical model, errors in the convective solution may distort the whole model because of the faulty baroclinic forces (arising from a faulty density distribution) which act in the equations of motion. The question is, whether the numerical smoothing of sharp density jumps still allows for an adequate solution of the dynamics.

In the present paper, a new method for solving the convection equation is described, where the above mentioned numerical errors are reduced drastically. The numerical solution is compared to a semi-analytic one, ensuring the quality of the numerical method. A few exemplary calculations, showing the influence of bottom friction, barriers, and tidal motion on the shape of the salt wedge, demonstrate the versatility of the numerical model.

2. Numerical Method

Figure 1 shows the schematic salt wedge and the geometry used in the present investigation. We take a channel of constant depth a and length S, open at both ends. The lateral (y-) dependence is neglected. The freshwater discharge Q enters from the right. The salt wedge is formed by the sharp density jump between salt water (density ρ_1) and fresh water (density ρ_0) at z = -t, the thickness of the wedge over the bottom is r.

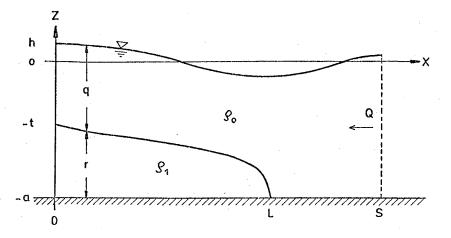


Figure 1. Salt wedge - schematic for definition of parameters.

DENSITY CURRENT MODEL

The numerical solution is based on the following equations: the equation of motion

$$\frac{\partial u}{\partial t} + \frac{1}{\rho} \frac{\partial p}{\partial x} - A \frac{\partial^2 u}{\partial z^2} = 0$$
(1)

the hydrostatic pressure equation

$$\frac{\partial p}{\partial z} + \rho g = 0 \tag{2}$$

the continuity equation for incompressible flow

$$\frac{\partial \mathbf{u}}{\partial \mathbf{x}} + \frac{\partial \mathbf{w}}{\partial \mathbf{z}} = \mathbf{0} \tag{3}$$

and the convection equation

$$\frac{\partial c}{\partial t} + u \frac{\partial c}{\partial x} + w \frac{\partial c}{\partial z} = 0$$
(4)

where the concentration c is related to the density ρ by

$$c = \frac{\rho - \rho_0}{\rho}$$
(5)

u and w are the velocities in the x- and z-direction, respectively. p is the pressure, g the gravitational acceleration, ρ the density, and \tilde{A} the vertical eddy viscosity coefficient. In (1), the convective terms have been neglected in order to make an analytic solution possible which is needed for the comparison purpose. Eq. (1) still contains the terms responsible for tidal motion and salt wedge formation , and major effects from the convective terms should only be expected near the tip of the salt wedge where the velocity gradient is large. It will be shown that this is the region where the numerical errors are largest, but the comparison to experimental salt wedge profiles is good, so the neglect of the convective terms can be justified. In eq. (4) the diffusion terms were neglected for the same reason, i.e. the desired analytical solution works with two fluid layers of different density as depicted in fig. 1, while diffusion would create a continuous vertical density profile. For the numerical model, a certain amount of numerical diffusivity cannot be avoided, and an additional physical diffusion term would make the comparisons even more difficult.

For the numerical solution of the dynamic equations (1-3) the scheme of Suendermann |12| was used. The linearized equations are solved by an explicit leap - frog method, whereby the z-dependency of the velocity u is treated implicitly. The time-step of this procedure is limited by the step size along the x-axis through the Courant stability criterion.

For the numerical solution of the convection equation, a newly developed method was applied |13|. For simplicity, the method is explained for the one-dimensional case. The spatial density distribution is represented by Hermite interpolation functions; at the computational grid points, the density value ρ_j and its local gradient $(\frac{\partial \rho}{\partial \mathbf{x}})_j$ are defined as timedependent variables. For example, the density representation between grid points 0 and 1 is given by

$$\rho(\mathbf{x}) = \rho_0 \mathbf{a}(\mathbf{x}) + \rho_1 \mathbf{b}(\mathbf{x}) + (\frac{\partial \rho}{\partial \mathbf{x}})_0 \mathbf{c}(\mathbf{x}) + (\frac{\partial \rho}{\partial \mathbf{x}})_1 \mathbf{d}(\mathbf{x})$$
(6)

with the Hermite interpolation polynomials

$a(x) = 2x^{3} - 3x^{2} + 1$	$b(x) = -2x^3 + 3x^2$		
$c(x) = x^{3} - 2x^{2} + x$	$d(x) = x^3 - x^2$	(7)	

This representation has the following properties

$$\rho$$
 (o) = ρ_0 , $\rho(1) = \rho_1$, $\frac{\partial \rho}{\partial x}$ (o) = $(\frac{\partial \rho}{\partial x})_0$, $\frac{\partial \rho}{\partial x}$ (1) = $(\frac{\partial \rho}{\partial x})_1$

The convection equation

$$\frac{\partial \rho}{\partial t} = -u \frac{\partial \rho}{\partial x}$$
(8)

is converted to the explicit difference equation

$$\rho_{j}^{n+1} = \rho_{j}^{n} - u_{j} \Delta t \left(\frac{\partial \rho}{\partial x}\right)_{j}^{n}$$
(9)

with j the spatial index and n the time-index, Δt is the time step.

For the gradient variables, another marching equation is needed. This equation is obtained from eq. (8) by spatial differentiation:

$$\frac{\partial}{\partial t} \left(\frac{\partial \rho}{\partial x} \right) = -u \frac{\partial^2 \rho}{\partial x^2} - \frac{\partial u}{\partial x} \frac{\partial \rho}{\partial x}$$
(10)

and transformed to the difference equation

$$\begin{pmatrix} \frac{\partial \rho}{\partial x} \end{pmatrix}_{j}^{n+1} = \begin{pmatrix} \frac{\partial \rho}{\partial x} \end{pmatrix}_{j}^{n} - \frac{u_{j}}{\Delta x} \begin{cases} \frac{6}{\Delta x} (\rho_{j-1}^{n} - \rho_{j}^{n}) + 4 \left(\frac{\partial \rho}{\partial x} \right)_{j}^{n} + 2 \left(\frac{\partial \rho}{\partial x} \right)_{j-1}^{n} \\ \frac{6}{\Delta x} (\rho_{j+1}^{n} - \rho_{j}^{n}) - 4 \left(\frac{\partial \rho}{\partial x} \right)_{j}^{n} - 2 \left(\frac{\partial \rho}{\partial x} \right)_{j+1}^{n} \end{cases}$$
(11)
$$- \frac{u_{j+1} - u_{j-1}}{2 \Delta x} \left(\frac{\partial \rho}{\partial x} \right)_{j}^{n}$$

where Δx is the spatial step size. The second term in the right-hand side of eq. (11) models the term $\frac{\partial^2 \rho}{\partial 2}$ and is obtained from the evaluation of the second derivative $\hat{\Phi}^x$ of eq. (6), letting $x \longrightarrow o$; upstream differences are taken in eq. (11), where the upper line holds for $u_1 > o$, the lower line for $u_1 < o$. The third term on the r-h-s of eq. (11) is a spatial nonlinear term and was omitted in the calculations because of its destabilizing behaviour. It was found that eqs (9) and (11) together are linearly unstable, but stability could be achieved by a small correction to eq. (9). Instead of eq. (8), the

$$\frac{\partial \rho}{\partial t} = - u \frac{\partial \rho}{\partial x} + \frac{u^2}{2} \frac{\Delta t}{\partial x^2}$$
(12)

was evaluated, where the corrective second term could immediately be taken from eq. (11).

The accuracy of the above described convective solution method is compared to serveral other methods in figure 2.

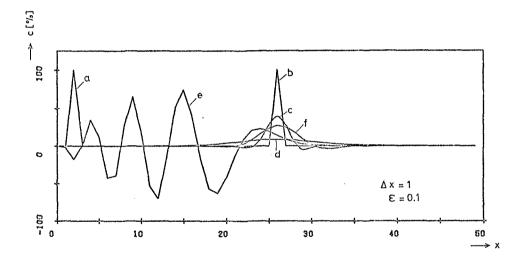


Figure 2. Numerical solution for convection of density spot. a) Initial, b) final density distribution (exact), c) present method, d) upstream differencing, e) forward time-centered space, f) Fromm's method.

As test example, the convection of a narrow density spot (initial width = $1.\Delta x$) over a distance $24.\Delta x$ was calculated by iterating over 240 time steps. The best approximation to the exact final density distribution is given by the present

COASTAL ENGINEERING-1976

method, which is even superior to the higher order method of Fromm |11|. The unstable character of the Forward Time-Centered Space method results in the strongly occillating curve, while the Upstream Differencing scheme displays the strong numerical damping. Many other methods like Leapfrog, Lax-Windroff, Finite Elements or Flux-Corrected Transport can be shown to be inferior to the method of Fromm |13|; the present method gives comparatively very good results, uses simple boundary conditions and needs little numerical effort, only some more core space is needed for storing the gradient values.

In two dimensions, a second expression analogous to eq. (11) has to be evaluated numerically. The calculation can be done by fractional time steps, scanning through the coordinate directions successively, or by computing and adding the contributions from both coordinates simultaneously; the latter method was used here.

3. Semi - Analytic Solution to the Stationary Salt Wedge

Omitting the partial time derivative in eq. (1), a quadratic zdependency of the velocity u can be obtained for each density layer (see fig. 1) separately, by integration. The non-slip condition is applied at the bottom:

u(-a) = 0 (13)

The total flow across r is zero:

$$\int_{-a}^{-t} u(z) dz = 0$$
(14)

(15)

Introducing the "baroclinic water level" k:

k(x) = h(x) - cq(x),

one gets for the velocity in the lower saline layer

 $u(z) = \frac{g}{6a} \frac{\partial k}{\partial x} \{ 3z^2 + 2 (2a + t) z + a (a + 2t) \}$ (16)

For the upper layer, the following two conditions are applied:

- 1.) the velocity u (z) must be continuous at the interface z = -t.
- 2.) The total fresh water flow across q has the given constant value Q:

$$\int_{-t}^{n} u(z) dz = Q$$
(17)

For the velocity in the upper layer one gets

$$u(z) = \frac{g}{2A} \frac{\partial h}{\partial x} z^{2} + \frac{1}{3} \left\{ \frac{g}{A} \frac{\partial h}{\partial x} (2t - h) - \frac{g}{A} \frac{\partial k}{\partial x} \frac{r^{2}}{q} + \frac{6Q}{q^{2}} \right\} z$$

$$+ \frac{1}{6} \left\{ \frac{g}{A} \frac{\partial h}{\partial x} t (t - 2h) + \frac{g}{A} \frac{\partial k}{\partial x} \frac{r^{2}}{q} (h - t) + \frac{12}{q^{2}} t \right\}$$
(18)

For the calculation of the wedge shape t(x) and the surface h(x) two conditions are needed. They are obtained by considering the tangential forces:

1.) the stress at the surface is zero

$$\frac{\partial u}{\partial z} \Big|_{z=h} = 0$$
(19)

2.) the stress at the interface is continuous

$$\frac{\partial u}{\partial z}\Big|_{z=-t=0} = \frac{\partial u}{\partial z}\Big|_{z=-t=0}$$
(20)

Inserting (16) in (20) and (18) in (19) and (20), one gets

$$\frac{\partial t}{\partial x} = \frac{1}{c} \frac{\partial h}{\partial x} \left(\frac{3}{2} \frac{h+t}{a-t} + 1 - c \right)$$
(21)
$$\frac{\partial h}{\partial t} = \frac{12}{c} \frac{QA}{QA}$$
(22)

$$\frac{dh}{\partial x} = -\frac{1}{g(h+t)^2} \frac{(4h+3a+t)}{(4h+3a+t)}$$
(22)

This system of nonlinear.first - order differential equations was solved (to an arbitrary degree of accuracy) by numerical methods, and the solution is referred to as semi - analytic.

Dimensional analysis of (21) and (22) shows that x scales with a⁴ while t and h scale with a, thereby establishing an affine relationship. Integrating (21) over the length L of the salt wedge gives the proportionality

$$L \sim \frac{gc}{QA} a^4$$
 (23)

where the remaining constant depends only on the relative depth of the salt wedge at the river mouth. Introducing the densimetric Froude- and Reynolds-numbers

$$Fr = \frac{Q}{\sqrt{cga^3}}$$
, $Re = \frac{\sqrt{cga^3}}{A}$

one has

$$L \sim \frac{Re}{Fr} a$$
 (24)

while the corresponding results of Keulegan |7| read

$$L \sim \frac{Re^{\frac{\pi}{4}}}{Fr^{\frac{5}{2}}} a$$
 (25)

for natural rivers and

$$L \sim \frac{Re^{T}}{Er^{\frac{5}{2}}} a$$

1

(26)

for hydraulic model flumes.

The difference in the results may arise from the simplifications in our theory, especially the constant eddy viscosity A and the non - slip condition (13).

4. Numerical Results

The computer code developed for the calculations permits the choice of variable step sizes in the vertical direction, variable bottom friction and bottom topography, and wind stresses at the surface. At the open boundaries upstream and downstream, the density distribution was kept fixed during the calculation. Care was taken that the salt wedge did not reach the upstream boundary. Since the bouyancy forces had been omitted in the initial differential equations, the hydrodynamically stable stratification had to be readjusted by averaging when a higher density value occurred above lower density values.

The fresh water discharge Q was taken as a dependent variable. As upstream and downstream boundary conditions the water levels were kept fixed. Stationary solutions were obtained after 10 000 time steps ($\triangleq 4$ weeks model time). The uniqueness of the solution was checked by starting from various density distributions; up to some minor differences in the velocity distribution, the same results were obtained in every case. More details of the calculations can be found in [14].

The following parameters were used throughout the calculations:

- Channel length s = 36 km, height a = 13.7 m
- Salt wedge thickness at the downstream end = 6.8 m, concentration = 3%

- Eddy viscosity coefficient $A = 10^{-3} m^2/s$

- Water levels upstream 4.7 cm, downstream 0.0 cm.

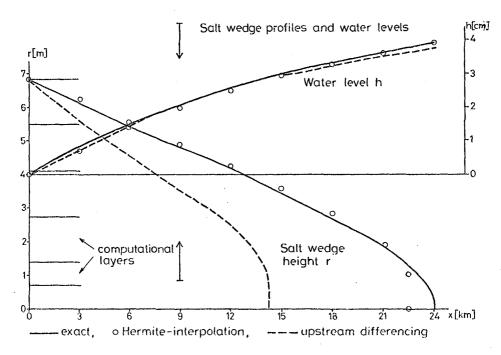


Figure 3. Stationary salt wedge profiles and water levels

Figure 3 shows the stationary salt wedges, computed by the various methods. For the present numerical method called "Hermite-interpolation", the 1.5% - isohaline was plotted as salt wedge boundary. The comparison to the semi-analytic curve called "exact" is good, major differences occur only at the tip of the wedge (where the neglect of the convective terms may play a significant role). It should be noted, however, that the wedge thickness in this region is comparable to the vertical grid spacing, as indicated in the figure. For comparison, another numerical solution is shown where the convection equation was solved by "upstream differencing". From this one can conclude that only the numerical high - precision solution of the field of highly stratified estuaries. The differences in the water level are less important, as shown in the upper part of the figure.

At x = 9 km, the vertical density profiles of the three different solutions are shown in figure 4.

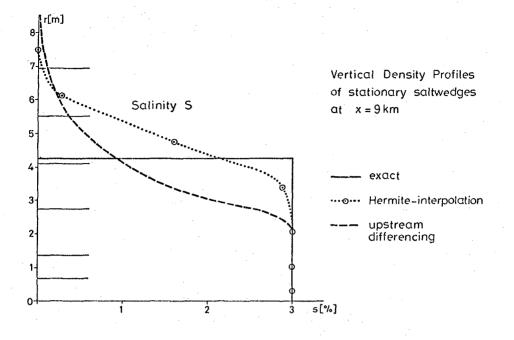
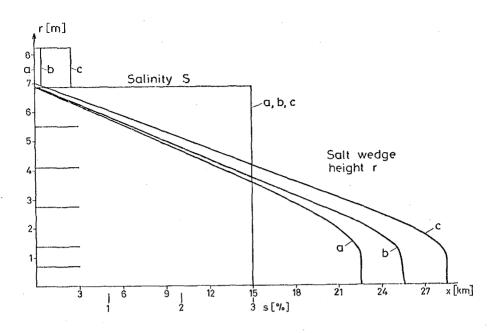


Figure 4. Vertical density profiles of stationary salt wedges from fig. 3. at x = 9 km

The sharp density jump of the exact representation is reproduced fairly well by the "Hermite-interpolation" method, while the "upstream differencing" - result shows a very long tail extending towards the channel surface.

All of the following numerical results are obtained with the method of "Hermite-interpolation". Figure 5 shows the changes in the shape of the salt wedge, when the density profile at the river mouth is altered.



<u>Figure 5.</u> Vertical salinity profiles at river mouth x = 0and corresponding salt wedges

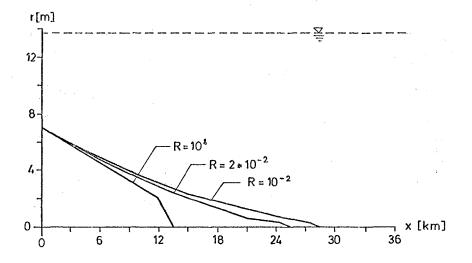
From this figure one can see that little changes in the river mouth density cause substantial changes in the wedge length. This high sensibility of the baroclinic model will make the calibration of parameters in a realistic calculation easier, and it might be interesting to observe such an effect in natura.

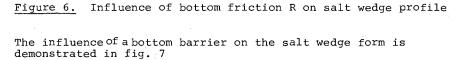
Figure 6 shows the influence of bottom friction on the salt wedge shape; the dimensionless friction coefficient R is defined by the Taylor formula for the bottom stress

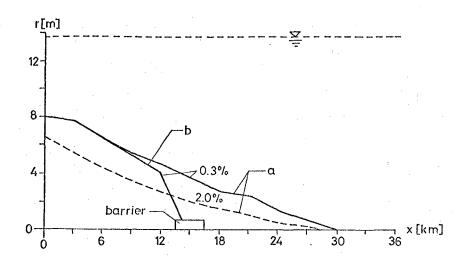
$$\tau = R u_{b} |u_{b}|$$

(27)

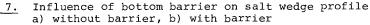
where u, is the bottom velocity. With decreasing bottom friction the length of the salt wedge increases. One could have thought of an increased fresh water discharge (because of the decreased bottom friction) and a corresponding shortening of the salt wedge length (see eq. 23), but the opposite is true.









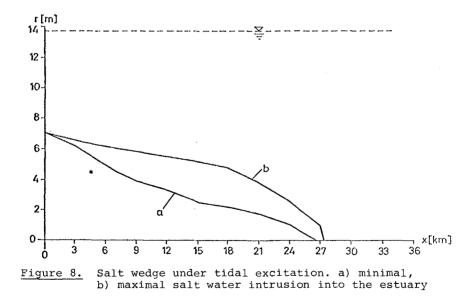


As can be seen in the figure, a barrier height d which is about 1/3 of the undisturbed salt wedge height, is fully sufficient to prevent the salt wedge from spreading out upstream. This result is contrary to Keulegan's |7| statement that the barrier must be as high as the salt wedge. The problem can be elucidatet by considering the velocity distribution eq. 16. For the lower two thirds of the wedge height r, the fluid moves upstream. No salt water can be transported upstream across a barrier of height d = 2r/3, because the transport velocity above this level is downstream. In addition, the velocity profile near the bottom is changed by a barrier, so that a barrier height of only r/3 prohibits salt intrusion.

As a first instationary calculation, a tidal wave was superimposed on the fresh-water discharge. The data for the calculation are:

		upstream		downstream	
	average water levels:	5.3	cm	0	cm
-	tidal amplitude:	102.8	cm	102.8	cm
-	tidal phase shift:	25.0	deg.	0	deg.
-	salt wedge thickness:			7.0	m

The calculation was carried out until periodic conditions were obtained. Figure 8 shows the salt wedges at high and low water. The difference in length is not large, but the



COASTAL ENGINEERING-1976

difference in salt wedge volume is. The constant height of the salt wedge at the downstream end is an unrealistic boundary condition and should be replaced by a tidally varying one. An indication of a computational instability was found near the tip of the wedge where the concentration at a single grid point was slowly but steadily increasing during the tidal periods. This effect can certainly be removed by more realistic boundary conditions and shall be further observed.

Finally, in order to show the relation of the present calculations to experimental data, the semi-analytic salt wedge curve is compared to Keulegan's |7| affine curve in figure 9.

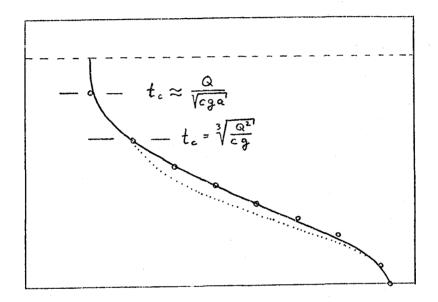


Figure 9. Comparison of semi-analytic salt wedge(full line) to experimental data. Dotted line: Keulegan's salt wedge |7|, fitted to critical flow conditions at river mouth Circles: Keulegan's salt wedge, fitted to present results Dashed line: Water surface

Taking the point of critical flow in the fresh water layer as "river mouth",

$$t_c = \sqrt[3]{\frac{Q^2}{cg}}$$

(28)

the dotted curve, taken from Keulegan's table |7|, should be compared to that piece of the semi-analytic solution curve covering the same x - interval. The comparison is rather bad, however, the relation (28) is based on homogeneous flow in both fluid layers and not very well justified experimentally |7|. Relaxing this condition and fitting Keulegan's curve (circles in fig. 9) to the present one, a very good comparison is obtained; the empirical critical depth for this case is

$$t_c \approx \frac{Q}{\sqrt{cga}}$$

(29)

In conclusion, the present numerical model appears to be well suited to calculate the hydrodynamics of highly stratified estuaries. Of course, the numerical problems in calculating partially mixed estuaries are comparatively small. The results of such a calculation are given in figure 10.

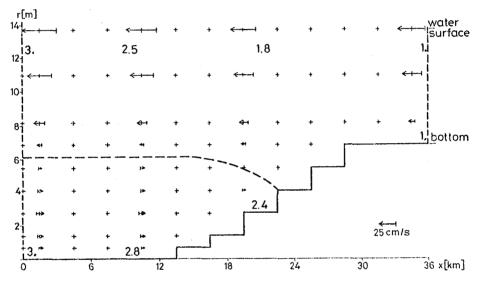


Figure 10. Horizontal velocities (arrows) and salinities (numbers) in a well - mixed estuary (stationary). Dashed line separates regions of upstream and downstream currents.

For this calculation, a horizontal and a vertical diffusion term were added to the density transport equation (4). The diffusion coefficients were taken as large as allowed by stability conditions for an eyplicit difference scheme. At the boundaries fully mixed conditions were prescribed (numbers indicate density values). The partial stratification in the interior had developed dynamically. The combined effects of longitudinal stratification and sloping bottom lead to a zone of upstream current velocity, indicated in the lower left part of the figure. This upstream current apparently exists independently from the degree of vertical stratification in the estuary, but only caused by the longitudinal stratification. The tip of the upstream current zone or equally the tip of the salt wedge are known to be the areas of maximum shoaling [3]. In consequence, for longitudinally stratified estuaries no information about the sediment transport can be obtained from measurements of surface velocities or calculations with vertically averaged numerical models, and this seems to hold for vertically stratified and mixed estuaries as well.

5. Summary and Conclusions

A numerical model for density currents in estuaries was presented, combining a classical solution scheme for the dynamical equations with a new solution scheme for the transport equation. The effects of baroclinic forces caused by density differences were studied in a two-dimensional x-z-model, and the results for a stationary salt wedge were shown to be in good agreement with a semi-analytic solution and experimental data. The uniqueness of the numerical solution was checked by varying the initial and boundary conditions. The influence of bottom friction, a bottom barrier, and tidal motions were studied; and the stationary solution for a well - mixed estuary was obtained.

It was found that the accuracy of the results for stratified estuaries depends mainly on the quality of the convective solution scheme, and that the present method of "Hermite-interpolation" gives satisfactory results in every case. As a practical aspect, it was found that bottom barriers for preventing salt intrusion into estuaries need not be as high as the undisturbed salt wedge. For realistic calculations, the time - dependency of water levels and vertical density profiles at the open ends of the estuary must be known from measurements.

6. Acknowledgements

The present work was done by funds of the Deutsche Forschungsgemeinschaft, Sonderforschungsbereich 79 (Wasserforschung im Küstenbereich). The major part of the numerical programming and production was done by W. P. Wittorf, student at Technische Universität Hannover. The support with computer programs and helpful discussions by J. Suendermann is gratefully mentioned.

References

- A.T. Ippen, "Salinity Intrusion in Estuaries", in |2|, chapter 13
- A.T. Ippen (ed.), "Estuary and Coastline Hydrodynamics", McGraw-Hill, New York 1966
- 3.) See [2], chapters 14, 15
- 4.) J.J. Dronkers, "Tidal Computations in Rivers and Coastal Waters", North-Holland Publ. Co., Amsterdam 1964, p. 18
- 5.) M.B. Abbott, J.A. Bertelsen, J.R. Warren, "Mathematical Modelling of Strorm Surges in Stratified Flow", Abstracts 15th Int. Conf. on Coastal Eng., Honolulu 1976, p. 1
- 6.) J.J. Leendertse, R.C. Alexander, S.K. Liu, " A Three-Dimensional Model of Estuaries and Coastal Seas. Vol. 1, Principles of Computation", Report R - 1417 - OWRR, Rand Corporation, 1973
- 7.) G.H. Keulegan, "The Mechanism of an Arrested Saline Wedge", in |2|, chapter 11
- 8.) F.A. Lee, Proc. ASCE Hydraul. Div. 100, 17 (1974)
- 9.) M. Rattray, E. Mitsuda, Estuarine and Coastal Marine Sci. 2, 375 (1974)
- 10.) B.P. Rigter, Proc. ASCE Hydraul. Div. 101, 765 (1975)
- 11.) J.E. Fromm, J. Comp. Phys. 3. 176 (1968)
- 12.) J. Suendermann, Mitt. Inst. Meereskunde Univ. Hamburg <u>19</u> (1971)
- 13.) K. Fischer, to be published
- 14.) W.P. Wittorf, Diplomarbeit, Techn. Univ. Hannover (1975), unpublished